Fabrication of Periodic Nanostructure Assemblies by Interfacial Energy Driven Colloidal Lithography

A. Dev, B. Dev Choudhury, A. Abedin, and S. Anand*

A novel interfacial energy driven colloidal lithography technique to fabricate periodic patterns from solution-phase is presented and the feasibility and versatility of the technique is demonstrated by fabricating periodically arranged ZnO nanowire ensembles on Si substrates. The pattern fabrication method exploits different interfaces formed by sol–gel derived ZnO seed solution on a hydrophobic Si surface covered by a monolayer of colloidal silica spheres. While the hydrophobic Si surface prevents wetting by the seed solution, the wedge shaped regions surrounding the contact point between the colloidal particles and the Si substrate trap the solution due to interfacial forces. This technique allows fabrication of uniform 2D micropatterns of ZnO seed particles on the Si substrate. A hydrothermal technique is then used to grow well-defined periodic assemblies of ZnO nanowires. Tunability is demonstrated in the dimensions of the patterns by using silica spheres with different diameters. The experimental data show that the periodic ZnO nanowire assembly suppresses the total reflectivity of bare Si by more than a factor of 2 in the wavelength range 400–1300 nm. Finite-difference time-domain simulations of the wavelength-dependent reflectivity show good qualitative agreement with the experiments. The demonstrated method is also applicable for other materials synthesized by solution chemistry.

1. Introduction

Colloidal lithography is an inexpensive, flexible, and efficient method for fabrication of two-dimensional patterns on large area.[1] This process is based on self-assembly of colloidal particles on a surface. Several strategies[2–5] have been developed to obtain a closed-packed monolayer arrangement of commercially available colloidal particles over a large-area. The void arrays, that is, the interstices in the close-packed arrangement are used to create 2D patterns either by depositing thin films by evaporation or sputtering or by etching the exposed substrate using a suitable anisotropic etching technique. Spherical colloidal particles with diameters ranging from tens of nanometers to several micrometers are commercially available; thus, a wide variety of patterns can be fabricated by colloidal lithography. The colloidal lithography technique has been extensively used to fabricate various periodic structures including nanowire/nanopillar arrays of different materials such as Si, ZnO, InP.[6–8] Despite being a very successful technique,[9] the use of colloidal lithography in case of wet-chemical synthesis has been very limited. The main limitation in using colloidal lithography in combination with solution-based synthesis is that the masked region, that is, the contact area between the colloidal sphere and the substrate is very small while the rest of the substrate remains accessible for the solution. So, in a normal approach involving drop casting of solution on a monolayer of colloidal particles, the solution easily penetrates through the interstices between the colloidal spheres and settles down on the substrate making a continuous layer with periodic holes.

With respect to pattern fabrication using liquids, superhydrophilic-superhydrophobic micropatterns is a unique and rapidly developing field, which is based on extreme differences in wettability between superhydrophilic and superhydrophobic regions on the same substrate.[10,11] Enormous research effort is being devoted to understand and control the wettability of the solid surface in order to uniquely and precisely control the geometry, position and the shape of the liquid droplets on the solid surface. In addition to the fabrication of periodic microdroplets,[10] this technique is also widely used in various other applications such as surface tension confined micro channels,[12] filling micro patterns,[13,14] passive dispensing by dewetting,[15] controlling bioadhesion,[16] cell encapsulation droplet arrays[17] and fabrication of complex micropatterns.[18] However, this technique is only suitable for large (>50 μm) structures.

Here, we combine colloidal lithography with generation of hydrophobic-hydrophilic regions and demonstrate a novel interfacial energy driven colloidal lithography technique to fabricate periodic micron and submicron-size patterns from solution phase. We utilize self-developed periodic wettability of a Si substrate in the presence of self-assembled colloidal silica spheres. The feasibility and the versatility of the concept are demonstrated by fabricating periodically arranged ZnO nanowire (NW) ensembles on sol–gel derived ZnO seed pattern

Dr. A. Dev, B. D. Choudhury, A. Abedin, Dr. S. Anand
School of Information and Communication Technology
KTH Royal Institute of Technology
Electrum 229, S-164 40, Kista, Sweden
E-mail: apurbad@kth.se

DOI: 10.1002/adfm.201400018

on Si substrates. The methods of growing ZnO NW ensembles on sol–gel seed layers have been investigated extensively and are well documented.[19–22] However, growing patterned arrays of ZnO NWs using colloidal lithography has mainly been demonstrated in case of vapor-phase methods.[8,23] Attempts to grow patterns of ZnO NWs ensembles using colloidal lithography and solution methods have not been very successful so far. Pyun et al.[24] reported formation of ZnO nanotube arrays when they used colloidal polystyrene (PS) sphere on ZnO seed layer. Fragala et al.[25] attempted to pattern ZnO seed by using monolayer of PS sphere arranged in a 2D arrays on Si substrate. By growing ZnO NWs on this patterned seed layer they realized an ordered array of Si holes spatially confined by ZnO NWs. In this article we demonstrate a pattern fabrication method that exploits different interfaces formed by sol–gel derived ZnO seed solution on hydrophobic Si substrate covered by monolayer of colloidal silica spheres. While the hydrophobic Si substrate prevents wetting by the seed solution, the wedge shaped region surrounding the contact point between the colloidal silica sphere and the Si substrate trap the solution due to interfacial forces. This method allows us to fabricate periodically arranged circular and ring-shaped patterns consisting of ZnO seed particles, on an area as large as several square centimeters. ZnO NWs were then grown on the generated seed patterns using a hydrothermal technique, resulting in well-defined periodic assemblies of ZnO NW bundles. Periodicity of the patterns was varied from 500 nm up to 3 μm using silica spheres with different sizes. The total reflectivity measurements were performed in order to investigate the interaction of these periodic structures with light. In the wavelength range 300–400 nm the reflectivity was less than 2%, resulting in enhanced absorption. In addition, compared to bare Si substrate the reflectivity is also significantly suppressed, by more than a factor of 2, for wavelengths 400–1300 nm. Finite difference time domain (FDTD) simulations of the wavelength dependent reflectivity show good agreement with the experimental data. The demonstrated method to obtain periodic patterns of ZnO seed-layer and ensembles of NWs is also applicable for other materials generated by solution chemistry, increasing the range of applications in optoelectronics and sensing.

2. Results and Discussions

Scanning electron microscopy (SEM) was performed after different fabrication steps. **Figure 1** shows representative SEM images of self-assembled silica spheres on a Si substrate. Figure 1a shows a large surface area uniformly covered with a monolayer (ML) of 3 μm silica spheres. Some domains with different sizes and position can be seen in Figure 1a. The reports in the literature[26] suggest that it is very challenging to achieve domain-free MLs. Domain size larger than few hundreds of micrometer is difficult to achieve. In case of self-assembly one of the inherent problems is that the commonly used colloidal particles, as in this work, often have a large size distribution. In addition, on a solid surface the dewetting of the solvent as well as the substrate roughness also influences the self-assembly process. With the self-assembly method used in this work, we have observed domain sizes within 100–300 μm. The results might be improved by using mono-disperse silica particles. As evident from Figure 1b, the colloidal spheres assemble in a hexagonal-close-packed (hcp) pattern, which is the most commonly observed pattern in self-assembled monolayers of colloidal spherical particles.[1] Wetting properties of the substrate also plays an important role in the self-assembly process on a solid substrate.[27] A good hydrophilic surface is necessary so that the colloidal suspension can homogenously spread on the substrate.[27] In our experiment, the Si substrates were first subjected to RCA 1 standard cleaning,[28] which improves the hydrophilicity of the silicon oxide surface. The procedure to form a monolayer of silica particles, as described in the experimental section, works very well for large particle sizes (>500 nm). High quality colloidal silica monolayers extending over ≈1 cm^2 were routinely obtained.

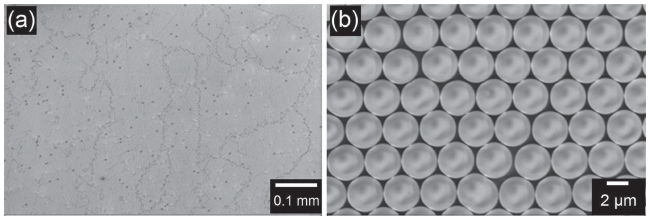

Figure 1. SEM images of a) the monolayer of silica spheres, which are hexagonally arranged b) magnified view.

The SEM images of periodically arranged ZnO seed patterns are presented in **Figure 2**. Figures 2a-d show the seed pattern fabricated by using 0.5, 1, 2, and 3 μm silica spheres, respectively. Insets in Figure 2a, c and d show magnified images of the corresponding samples. All the samples show fairly uniform circular-shaped seeded regions. Figure 2c,d show uniform seed patterns on a large area. The average diameter of the circular region of the ZnO seed layer varies as 0.3, 0.6, 1, and 2.1 μm as the diameter of the colloidal silica particle increases from 0.5 to 3 μm, whereas the period closely follows the diameter of the corresponding silica spheres. However, some variations in the diameter and period of the ZnO seed patterns can be seen in Figure 2c. Other samples also show similar variations, which we attribute to the size distribution of the colloidal particles. The hexagonal arrangement of the circular ZnO seed layer shows that the seed solution follows the hcp arrangement of the silica spheres.

Figures 3a,b show magnified SEM images of the circular seeded regions fabricated using 2 and 3 μm silica spheres, respectively. Three distinctly different concentric regions can be identified in each of these images. The center (e.g., region "a" in Figure 3a) remains mostly free of seed particles, followed by region "b" where some random clusters of white ZnO seed particles are visible. Finally, a relatively uniform ZnO seed layer coverage can be seen in the outer ring (region c). ZnO seed layers grown on samples with other silica sphere sizes (0.5 and 1 μm) also exhibit similar patterns. However, the relative widths of the different concentric regions, as depicted in Figure 3a, depend on the size of the colloidal particles. The average diameter of the region "a" increases from 85 nm to 350 nm as the colloidal particle size increases from 0.5 μm to 3 μm.

Figures 4a–c show the SEM images of hydrothermally grown ZnO NWs on the ZnO seed layer patterned by 1, 2, and 3 μm

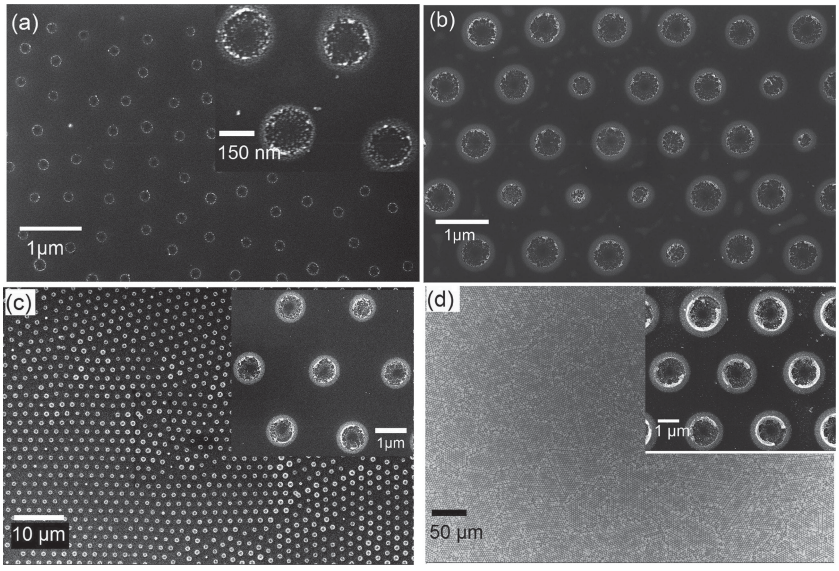

Figure 2. SEM images of ZnO seed patterns fabricated using a) 0.5 μm, b) 1 μm, c) 2 μm and d) 3 μm colloidal silica spheres. Insets show magnified images of corresponding samples.

silica spheres, respectively. As expected, the growth of ZnO NWs follows the periodic arrangement of the seed layer (patterns). Magnified images of the periodic ZnO NW ensembles are presented in Figures 4d–f. As the size of the colloidal particle increases the diameter of the central region (region "a" without any seed particles as shown in Figure 3a) also increases. This leads to the formation of ring-shaped pattern of ZnO NW patches as can be seen in Figures 4c,f. The lateral extents (diameters) of the NW ensembles are comparable to the corresponding seed pattern. In all samples, the grown ZnO NWs have hexagonal cross sections and their lateral size distribution is within 50–150 nm. The vertical orientation of the NWs improves as the size of the ZnO seed area increases.

The morphology and the crystalline quality of the as prepared ZnO nanowires were further investigated by transmission electron microscope (TEM). **Figures 5**a,b show typical TEM images of the fabricated NWs. Figure 5b shows some isolated NWs with a diameter of ≈50 nm. The high-resolution TEM (HRTEM) images taken from selected areas of Figure 5a,b are presented in Figure 5c,d. The clear lattice fringes demonstrate that the NWs are single crystalline. The interplanar spacing calculated from the HRTEM image is about 0.28 nm, which corresponds to the separation between $(01\bar{1}0)$ set of planes of hexagonal wurtzite ZnO crystal. Clearly, these planes are parallel to the axis of the nanowire indicating that the NWs grew along *c*-axis (<0001> direction), as usually observed in most of the synthesis methods reported in the literature.[19,20]

Formation of the seed pattern is the most important requirement in order to achieve periodic arrangements of ZnO NWs using the technique described here. Sol–gel technique is widely used to make homogeneous layers of ZnO films on different substrates. However, the stability of such a liquid film crucially depends on different interfacial forces as schematically depicted in **Figure 6**a. In air, the interfacial energy of the solid surface is usually described by the "surface energy" W_{SV}, whereas the liquid–air interface is described by the "surface tension" W_{LV}. When a liquid drop is placed on a solid surface, three interfaces are formed as shown in Figure 6a. The liquid drop will tend to spread on the surface if the combined interfacial energy of the liquid droplet (W_{LV} + W_{LS}) is less then the surface energy (W_{SV}) of the solid. Conversely, when the surface energy of the solid is low the surface is said to be stable and it will cause the liquid to bead up in order to maximize the free surface. The situation is usually described in terms of spreading pressure or spreading coefficient "*S*" defined as:[29]

$$S_{LS} = W_{SV} - (W_{LV} + W_{LS}) \quad (1)$$

A liquid will spread on a solid surface only for positive spreading pressure. High surface energy, or in other words a proper wettability of the substrate is thus required in order to achieve a homogeneous liquid film on it.

Due to their enormous technological importance, the wettability of Si surfaces has been extensively investigated.[30–34] A number of factors such as the absorbed molecules, surface oxide thickness, surface roughness, humidity etc. have been reported to influence the surface energy and hence the wettability of Si surfaces.[30,31,33] A suitable surface preparation procedure is thus necessary to obtain a homogeneous liquid film on Si surfaces. For growing ZnO thin films on Si using sol–gel technique, HF treatment or RCA 1 standard cleaning[28] is usually performed prior to the coating step. However, the wettability of the Si surfaces deteriorate over time, particularly in the presence of high humidity.[30] It is well known that an amorphous SiO_2 layer on Si absorbs water from the humid environment. At room temperature and at low relative humidity (RH) the absorbed water layer in SiO_2 is believed to form an ice-like monolayer, which helps in increasing the surface energy.[35,36] However, at high RH

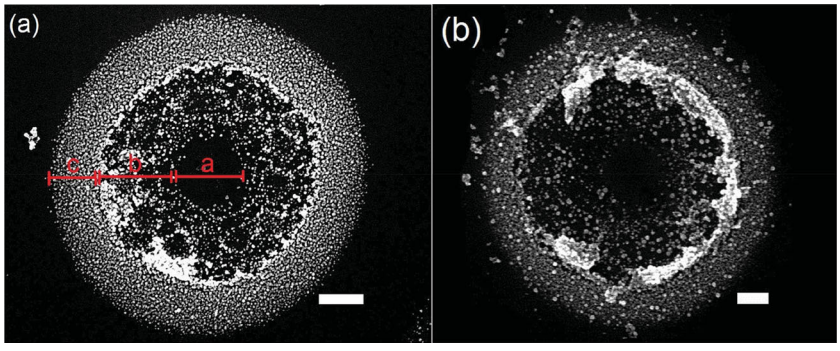

Figure 3. SEM images showing magnified views of circular ZnO seed patterns fabricated using a) 2 μm, b) 3 μm; scale bar in both images is 200 nm.

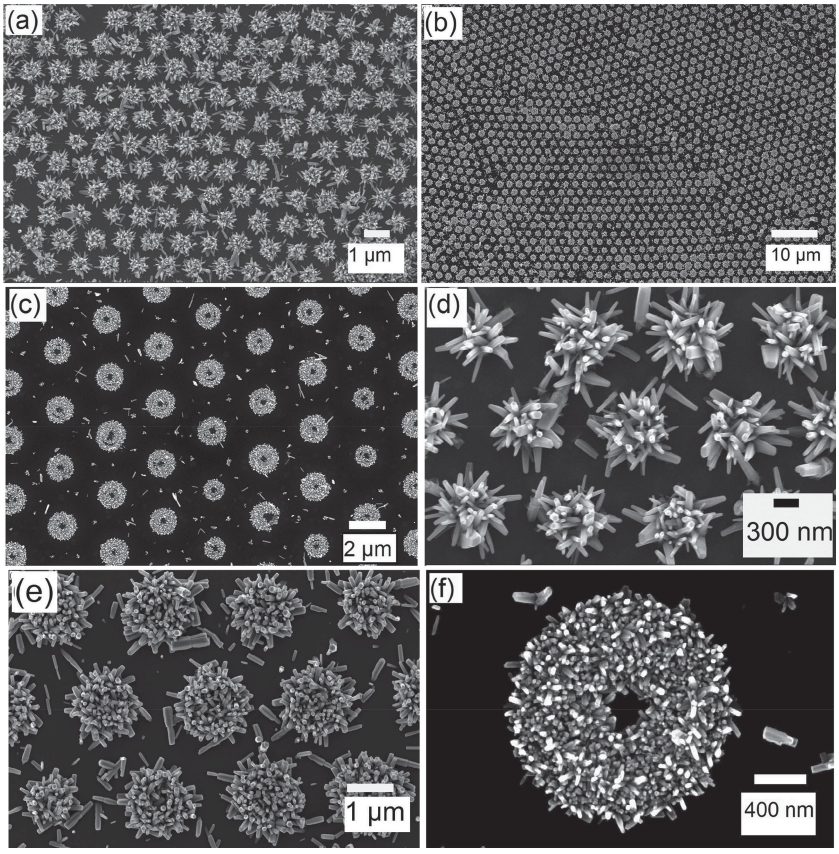

Figure 4. SEM images of ZnO NWs patterns fabricated using a) 1 μm, b) 2 μm, c) 3 μm. Magnified view of the corresponding samples are presented in d–f), respectively.

the structure of the absorbed water changes from ice to water which lowers the surface energy.[30,37] The freshly treated Si substrates used in the present investigation show good adhesivity with the ZnO seed solution. However, during deposition of the colloidal silica monolayer, as the substrate is kept in an aqueous solution for a long time (typically 2–3 h) the adhesivity of the substrate strongly reduces. This explains why the ZnO seed solution does not adhere to the exposed silicon substrate in between the colloidal spheres. In contrast, a completely different situation arises under the colloidal silica sphere and is schematically presented in Figure 6b. The wedge-shaped space in between the substrate and the colloidal sphere will effectively replace a major part of the air–liquid interface by a solid–liquid interface. In addition, the curved surface of the colloidal sphere reduces the contact angle of the liquid towards the centre (Figure 6b). As a result, the seed solution under the colloidal sphere forms a stable film.

Three distinct regions, as shown schematically in **Figure 7**, are expected in the ZnO seed pattern if the seed solution settles down on the substrate following the above model. At the center (region a) where the silica spheres are in close contact with the substrate, no seed particles are expected. Away from the center, a seed layer with gradually increasing thickness is expected (region b), where seed solution will be in contact with both the substrate and the colloidal particles. Finally, a more homogeneous region is expected in the outermost ring (region c) where the seed solution is in contact only with the substrate. Upon annealing, the seed layer crystalizes maintaining the generated shape and the pattern.

The hydrothermal growth of ZnO NWs in aqueous solution containing hexamethylenetetramine (HMT) and zinc nitrate is well documented in literature.[38–40] The patterned layer of ZnO seed crystals provides preferential sites for heterogeneous nucleation, which anisotropically grows leading to periodic pattern of single crystalline ZnO NW assemblies. The simple model presented above is in very good agreement with the experimental results (Figure 2,4) discussed earlier.

One of the key advantages of the fabrication method presented here is that the seed pattern only follows the pattern of the first layer of the colloidal silica spheres. Multilayer colloidal silica particles, if present, does not influence the seed pattern as long as the

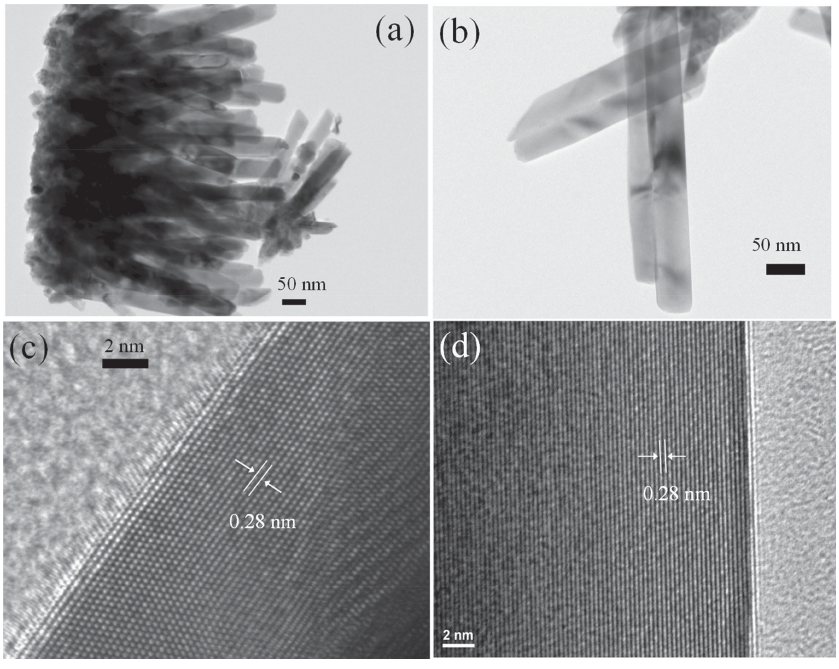

Figure 5. A typical TEM image of the fabricated ZnO NWs. a) A bunch of NWs and b) few isolated NWs. HRTEM image taken from a selected area (indicated by black square) of (a,b) are presented in (c,d), respectively.

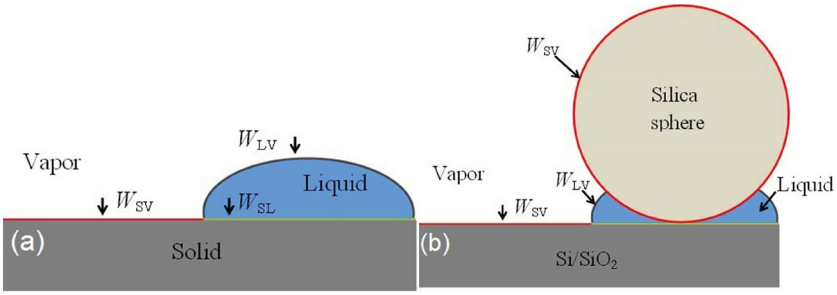

Figure 6. Schematic sketch showing different interfaces formed in the liquid–solid system: a) Between a liquid droplet and a flat solid surface, and b) between a liquid droplet and a flat solid surface in the presence of a colloidal silica sphere.

periodicity of the first layer is maintained. The method thus enables us to prepare periodically ordered arrays over a very large area. Such structures are very important for periodic modulation of refractive index (RI), which allows to design tunable light trapping structures. We performed total reflectivity measurements of the samples using a spectrophotometer (Perkin Elmer LAMBDA 950) equipped with a 150 mm integrating sphere. All the samples were illuminated with a beam condenser on a small spot of about 2 mm in diameter. Measurements taken at different parts of the samples show consistent results. The influence of the periodicity of the ZnO NW assemblies, on the reflectance spectra was analyzed. These results were compared with those obtained from bare Si substrates, Si substrates uniformly coated with ZnO seed layers and Si substrates densely covered with ZnO NWs (referred to as ZnO NW coated Si). The reflectance measurements are presented in **Figure 8**. As compared to the reference Si substrate (uncoated), ZnO NW coated Si shows a strong reduction in total reflectivity in the entire spectral range below 1000 nm. The drops at around 375 nm and 1100 nm are due to band edges of ZnO and Si, respectively. The reduction in reflectivity for ZnO NW coated Si is mainly due to presence of the low index ZnO (RI ≈ 2) in between Si (RI ≈ 3.5) and air. Previous studies also suggest a contribution from gradient index profile that might result from tapered profile of NWs as well as height variations.[6,41] Clearly, samples with periodic NW ensembles also exhibit similar low reflectivities below 1000 nm (Figure 8) despite the fact that the surface coverage of the NWs in case of periodic ensembles is less than 40% as compared to continuous NWs layer.

In addition, the samples with periodic ZnO NW ensembles exhibit better antireflection properties in the longer wavelength range (>1000 nm). Considering the larger spatial periodicity, the reduction in reflectivity cannot be explained by gradient index concept. However, for large structures the reflected and transmitted intensity can redistribute from the specular to the diffracted components increasing large angle diffuse scattering.[42,43] As a result, photons are trapped and coupled into the guided modes of the absorber due to total internal reflection occurring at large scattering angle.[44] To qualitatively understand the experimental results, reflectivity from similar structures were simulated using the Finite-difference time-domain (FDTD) method. A commercial FDTD software package (Lumerical) was used to simulate the total reflectivity of the different structures. For the simulation, each circular structure of the periodic ZnO NW ensembles was approximated by a cylinder having a length of 1 micron and diameters equal to the circular patches of the corresponding sample, that is, 0.3, 0.6, 1 or 2.1 μm for the patterns fabricated using 0.5, 1, 2, or 3 μm silica spheres, respectively. A hexagonal arrangement has been assumed (**Figure 9**b) with each cylinder having an effective refractive index of 1.8 to take into account the porous nature of the ZnO NW ensembles. On the other hand, the un-patterned ZnO NW arrays has been approximated by a dense array of ZnO cylinders in a hexagonal lattice with each ZnO cylinder having a length and diameter of 1 μm and 75 nm, respectively. The separation (center-to-center) between the cylinders was assumed to be 100 nm and refractive index of 2.0 (Figure 9d). In addition, a rough ZnO layer of 75 nm is assumed in between ZnO NWs and Si substrate in all cases to account for the residual ZnO seed layer in the actual samples. The refractive index and extinction coefficient for ZnO in the above wavelength range was used in the simulations. The simulated data for the total reflectivity vs. wavelength obtained for the different structures are shown in the **Figure 10**. Other than the strong interference fringes the simulated spectra show a similar trend as observed experimentally, for example the average reflectivity of about 10% from ZnO NW coated Si substrate in the wavelength range 400–1000 nm The interference fringes in the simulated spectra, in contrast to the smoother profiles observed experimentally (Figure 8), is mainly due to the flat top approximation of the NWs in the simulations, whereas the actual sample contains NW of varying heights and orientations. However, the overall trend in the investigated wavelength range shows good agreement with the experiment. The sharp drop in reflection at around 375 nm is due to the band edge absorption of ZnO. The strong interference fringes, however, subdue the expected drop in reflection close to Si band edge at around 1100 nm. The sharp increase in reflection at around 400 nm can be attributed to the material properties (refractive index and extinction coefficient) of ZnO. The behavior of the periodic structures in the longer wavelength (>1000 nm) also shows quite good agreement with the experiment with lower reflectivity as compared to the un-patterned sample. Considering their good antireflection properties in a large spectral window, such architectures may also be interesting for near infrared devices.

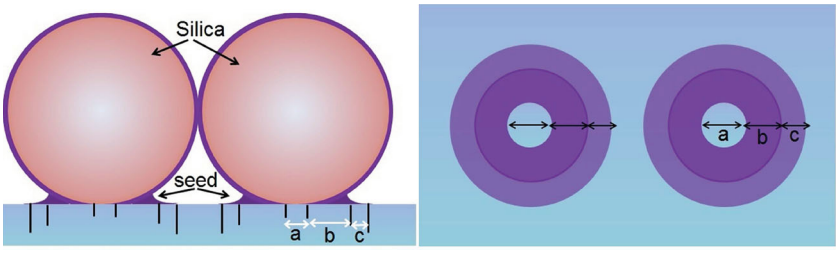

Figure 7. Schematic showing the origin of different concentric regions in circular ZnO seed patterns.

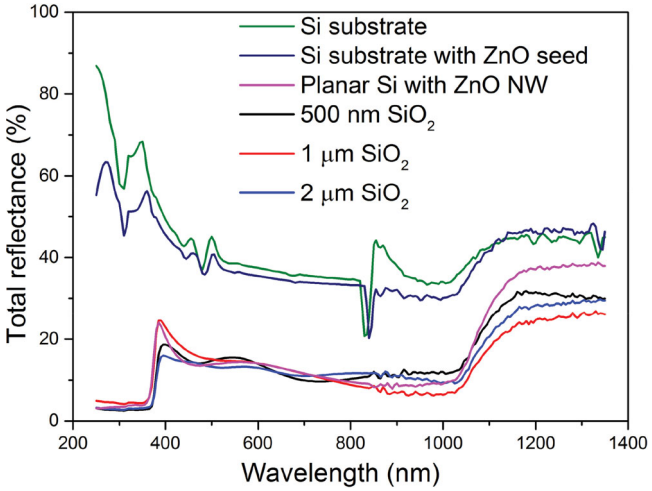

Figure 8. Total reflectance spectra of bare Si substrate and substrate covered with ZnO seed layer, continuous ZnO NW arrays and periodic ZnO NW assembly fabricated using 0.5, 1, and 2 μm SiO_2 particles.

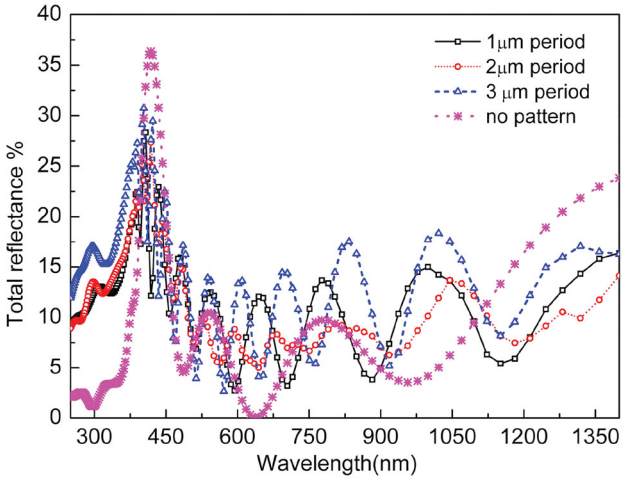

Figure 10. Simulated total reflectance spectra of Si substrate covered with continuous and periodic ZnO NW assemblies with 1, 2, and 3 μm periodicity.

3. Conclusion

In summary, we demonstrate a novel technique to fabricate 2D periodic patterns from solution by exploiting different interfaces formed between the solution, substrate and the self-assembled colloidal silica particles. The efficacy of the technique is demonstrated by fabricating circular and ring-shaped periodic assemblies of vertically aligned ZnO NW. Hexagonally arranged circular seed patterns were first formed on Si substrates by using sol–gel technique. As the hydrophobic Si substrate prevents wetting by the seed solution, the wedge shaped region below the colloidal particles facilitates wetting due to reduced air–liquid interface. The technique allows wafer-scale fabrication of 2D pattern from solution. We also demonstrate easy controllability of feature size and periodicity by using different sizes of colloidal silica sphere. The patterns can be further tuned by using isotropic etching of the hexagonally arranged colloidal silica particles. Considering the wide range of applications of such periodic structures for efficient photon management, total reflectivity of the samples was measured which shows strong suppression of reflectivity in a very large spectral window. The simulated reflectivity spectra obtained by FDTD simulations also show good qualitative agreement with the experiments. The simple fabrication process, combining colloidal lithography and solution synthesis, presented here can be adopted to fabricate periodic structures from a wide variety of materials, increasing the range of applications in optoelectronics and sensing.

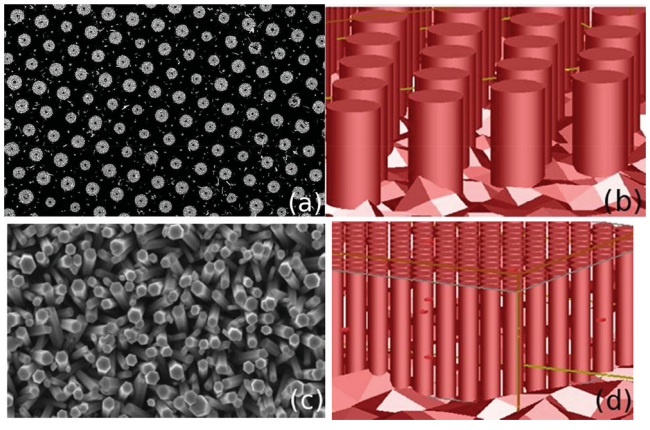

Figure 9. SEM images of representative sample, a) patterned assemblies of ZnO NW ensembles, c) continuous layer of ZnO NW arrays; Schematic showing the structure assumed for simulation b) patterned assemblies of ZnO NW ensembles, d) continuous layer of ZnO NW arrays.

4. Experimental Section

Colloidal lithography on silicon substrates: Silicon substrates were first cleaned following RCA 1 standard cleaning procedure.[28] The substrate were boiled for 15 min at 70 °C in an activation solution containing a mixture of H_2O_2 (30%), NH_4OH (30%), and DI water in a ratio of [1:1:5] and then rinsed in DI-water. An aqueous suspension of SiO_2 particles (Sigma Aldrich) was made with different concentrations of silica particles depending on the particle diameter and the substrate area. Silica spheres with four different diameters, 3, 2, 1, and 0.5 μm were used. The substrate was placed inside a glass petri dish slightly bigger than the substrate and the prepared colloidal suspension was dropped on it making the substrate completely submerged under the suspension. After a few hours, depending on the particle size, the silica particles settled down forming a monolayer on the substrate surface. The liquid remaining on the top of the substrate was then removed by a syringe, and the substrate was left to dry in air.

Patterned Seed Layer Preparation: For ZnO seed layer preparation, zinc acetate dehydrate [$Zn(CH_3COO)_2$, $2H_2O$] was dissolved in dry ethanol (100 mM). In order to make zinc acetate soluble in ethanol, a few droplets of diethanolamine (DEA) was added and then stirred for around 30 min. The solution was then spin-coated on the silicon substrates covered with a monolayer of silica spheres. The substrates were first dried on a hotplate at 80 °C and, then annealed in an oven at 400 °C in ambient air. The samples were sonicated in ethanol for about 30 seconds to remove the colloidal spheres from the surface.

Growth of Periodic ZnO Nanowire Assemblies: For the growth of ZnO NWs 50 mM zinc nitrate and 50 mM hexamethylene tetramine (HMT) were dissolved in 30 mL of DI-water. The samples were placed horizontally in a glassware with the seeded surface facing down. The

growth solution was added to the glassware and refluxed at 95 °C in an oil bath for one hour. Finally, after ZnO NW growth the samples were removed from the solution and rinsed in DI-water and dried under nitrogen flow.

Acknowledgements

The work was performed within the Linné center for advanced optics and photonics (ADOPT), and was supported by the Swedish Research Council (VR). Partial support from the European Union FP7 Network of Excellence Nanophotonics4Energy (N4E) and Nordic Innovation Center project NANORDSUN is acknowledged.

Received: January 3, 2014
Revised: February 21, 2014
Published online: April 22, 2014

[1] X. Ye, L. Qi, *Nano Today* **2011**, *6*, 608.
[2] A. S. Dimitrov, K. Nagayama, *Langmuir* **1996**, *12*, 1303.
[3] M. Trau, D. A. Saville, I. A. Aksay, *Science* **1996**, *272*, 706.
[4] X. Li, T. Wang, J. Zhang, X. Yan, X. Zhang, D. Zhu, W. Li, X. Zhang, B. Yang, *Langmuir* **2010**, *26*, 2930.
[5] S.-M. Yang, S. G. Jang, D.-G. Choi, S. Kim, H. K. Yu, *Small* **2006**, *2*, 458.
[6] B. D. Choudhury, A. Abedin, A. Dev, R. Sanatinia, S. Anand, *Opt. Mater. Express* **2013**, *3*, 1039.
[7] S. Naureen, R. Sanatinia, N. Shahid, S. Anand, *Nano Lett.* **2011**, *11*, 4805.
[8] Wang Wang, C. J. Summers, Z. L. Wang, *Nano Lett.* **2004**, *4*, 423.
[9] H. W. Deckman, J. H. Dunsmuir, *Appl. Phys. Lett.* **1982**, *41*, 377.
[10] E. Ueda, P. A. Levkin, *Adv. Mater.* **2013**, *25*, 1234.
[11] P. Ferraro, S. Coppola, S. Grilli, M. Paturzo, V. Vespini, *Nat. Nanotechnol.* **2010**, *5*, 429.
[12] M. J. Hancock, J. He, J. F. Mano, A. Khademhosseini, *Small* **2011**, *7*, 892.
[13] J. S. Li, E. Ueda, A. Nallapaneni, L. X. Li, P. A. Levkin, *Langmuir* **2012**, *28*, 8286.
[14] D. Zahner, J. Abagat, F. Svec, J. M. J. Fréchet, P. A. Levkin, *Adv. Mater.* **2011**, *23*, 3030.
[15] E. Ueda, F. L. Geyer, V. Nedashkivska, P. A. Levkin, *Lab. Chip* **2012**, *12*, 5218.
[16] F. L. Geyer, E. Ueda, U. Liebel, N. Grau, P. A. Levkin, *Angew. Chem. Int. Ed.* **2011**, *50*, 8424.
[17] A. I. Neto, C. A. Custódio, W. Song, J. F. Mano, *Soft Matter* **2011**, *7*, 4147.
[18] M. J. Hancock, F. Yanagawa, Y.-H. Jang, J. He, N. N. Kachouie, H. Kaji, A. Khademhosseini, *Small* **2012**, *8*, 393.
[19] S. Xu, Z. L. Wang, *Nano Res.* **2011**, *4*, 1013.
[20] A. Dev, S. K. Panda, S. Kar, S. Chakrabarti, S. Chaudhuri, *J. Phys. Chem. B* **2006**, *110*, 14266.
[21] L. Vayssieres, *Adv. Mater.* **2003**, *15*, 464.
[22] L. E. Greene, B. D. Yuhas, M. Law, D. Zitoun, P. Yang, *Inorg. Chem.* **2006**, *45*, 7535.
[23] D. F. Liu, Y. J. Xiang, X. C. Wu, Z. X. Zhang, L. F. Liu, L. Song, X. W. Zhao, S. D. Luo, W. J. Ma, J. Shen, W. Y. Zhou, G. Wang, C. Y. Wang, S. S. Xie, *Nano Lett.* **2006**, *6*, 2375.
[24] Y. B. Pyun, J. Yi, D. H. Lee, K. S. Son, G. Liu, D. K. Yi, U. Paik, W. I. Park, *J. Mater. Chem.* **2010**, *20*, 5136.
[25] M. E. Fragalà, Y. Aleeva, G. Malandrino, *Superlattices Microstruct.* **2010**, *48*, 408.
[26] X. M. Lin, H. M. Jaeger, C. M. Sorensen, K. J. Klabunde, *J. Phys. Chem. B* **2001**, *105*, 3353.
[27] N. Vogel, *Surface Patterning with Colloidal Monolayers*, Springer, Heidelberg **2012**.
[28] G. K. Celler, D. L. Barr, J. M. Rosamilia, *Electrochem. Solid-State Lett.* **2000**, *3*, 47.
[29] D. Bonn, J. Eggers, J. Indekeu, J. Meunier, E. Rolley, *Rev. Mod. Phys.* **2009**, *81*, 739.
[30] X. Xi, J. Shi, S. Maghsoudy-Louyeh, B. R. Tittmann, *AIP Conf. Proc.* **2010**, *1211*, 1493.
[31] B. Olbrechts, X. Zhang, Y. Bertholet, T. Pardoen, J.-P. Raskin, *Microsyst. Technol.* **2005**, *12*, 383.
[32] M. C. Gomes, A. C. Fernandes, B. S. Almeida, R. M. Almeida, *J. Mater. Sci.* **1995**, *30*, 3893.
[33] D. Janssen, R. De Palma, S. Verlaak, P. Heremans, W. Dehaen, *Thin Solid Films* **2006**, *515*, 1433.
[34] E. J. Chibowski, *Adv. Colloid Interface Sci.* **2005**, *113*, 121.
[35] A. Verdaguer, C. Weis, G. Oncins, G. Ketteler, H. Bluhm, M. Salmeron, *Langmuir* **2007**, *23*, 9699.
[36] I. M. P. Aarts, A. C. R. Pipino, J. P. M. Hoefnagels, W. M. M. Kessels, M. C. M. van de Sanden, *Phys. Rev. Lett.* **2005**, *95*, 166104.
[37] D. B. Asay, S. H. Kim, *J. Chem. Phys.* **2006**, *124*, 174712.
[38] Z. Zhou, Y. Deng, *J. Phys. Chem. C* **2009**, *113*, 19853.
[39] B. Weintraub, Y. Deng, Z. L. Wang, *J. Phys. Chem. C* **2007**, *111*, 10162.
[40] H.-H. Park, X. Zhang, K. W. Lee, K. H. Kim, S. H. Jung, D. S. Park, Y. S. Choi, H.-B. Shin, H. K. Sung, K. H. Park, H. K. Kang, H.-H. Park, C. K. Ko, *CrystEngComm* **2013**, *15*, 3463.
[41] M. Coakley, *Growth and Optical Characterization of Zinc Oxide Nanowires for Anti-reflection Coatings for Solar Cells*, Thesis, Portland State University, **2011**.
[42] H. Shimomura, Z. Gemici, R. E. Cohen, M. F. Rubner, *ACS Appl. Mater. Interfaces* **2010**, *2*, 813.
[43] C. Martella, D. Chiappe, P. D. Veneri, L. V. Mercaldo, I. Usatii, F. B. de Mongeot, *Nanotechnology* **2013**, *24*, 225201.
[44] F.-J. Haug, K. Söderström, A. Naqavi, C. Ballif, *J. Appl. Phys.* **2011**, *109*, 084516.

